

1 **On the set of deterministic phenomena preceding the earthquake June  
2 25, 2021 with a magnitude of 5.4 near the city of Yayladere (Turkey)**

3 **Alexandr Volvach<sup>1</sup>, Lev Kogan<sup>2</sup>, Konstantin Kanonidi<sup>3</sup>, Igor Bubukin<sup>4</sup>, Valeria Shtenberg<sup>2</sup>,  
4 Larisa Volvach<sup>1</sup>**

5 <sup>1</sup>Radio Astronomy and Geodynamics Department of Crimean Astrophysical Observatory, Katsiveli, RT-22 Crimea

6 <sup>2</sup>Nizhny Novgorod State University of Architecture and Civil Engineering, Nizhny Novgorod, Russia

7 <sup>3</sup>Pushkov Institute of Terrestrial Magnetism, Ionosphere and Radiowave Propagation of RAS, Moscow, Russia

8 <sup>4</sup>Radiophysical Research Institute of N.I. Lobachevsky Nizhny Novgorod State University, Nizhny Novgorod, Russia

10 *Correspondence to:* Alexandr E. Volvach (volvach@meta.ua)

11 **Abstract.** The article examines the 5.4 magnitude earthquake that occurred on June 25, 2021 in the vicinity of Yayladere  
12 (Turkey). The analysis of the geomagnetic measurements carried out revealed a set of deterministic processes that preceded  
13 this event and are interpreted as its precursors. An estimate is made of the average time between the interval of existence of  
14 such phenomena and the moment of the earthquake under consideration. As a result, close values of the corresponding averaged  
15 time intervals were obtained for the statistics of all three components of the geomagnetic field considered in the article. The  
16 proposed technique can be used to predict seismic processes in various regions of the world in a near real-time mode.

17 **1 Introduction**

18 During the last years a number of scientists published the results of researches, indicative of possibility of registration of  
19 harbingers of strong earthquakes in the distance of more than 5000 km, and in some cases more than 10 000 km (Hasanov &  
20 Keramova 2006; Lyubushin 2008; Sobolev et al. 2008; Khain and Khalilov 2008).

21 Philosophy of short-term forecasting of earthquakes hasn't undergone essential changes during the whole history of its  
22 presence. The basis of all technologies of short-term forecasting the earthquakes is to create the network of stations, which  
23 register the changes of geophysical, geochemical, hydro-geological and other parameters of geological medium before strong  
24 earthquakes near potential sources of possible earthquakes.

25 This article discusses deterministic processes that were detected in the last few hours before an event with a magnitude of  $M$   
26 = 5.4 with an epicenter of  $39.196^{\circ}$  N,  $40.165^{\circ}$  E, which occurred at 18:28:37 (UTC) on 25.06.2021, 8 kilometers from the city  
27 of Yayladere (Turkey). The object of the study was the statistics of magnetic field measurements carried out at the test site of  
28 the Radio Astronomy and Geodynamics Department of the Crimean Astrophysical Observatory in Katsiveli (Crimea) during  
29 the period 00:00:00 on 24.06.2021 – 23:59:59 on 25.06.2021. In order to search for precursors of an impending earthquake,  
30 the technique proposed in (Volvach et al. 2022a,b,c,d; Volvach et al. 2023; Kogan et al. 2021; Kogan 2015)<sup>1</sup> and based on the

31 change in the properties of the probability density of any random process when even a very small term appears in its  
32 composition, the nature of which is weakly related to a set of commonly occurring phenomena, was applied.  
33 As will be shown below, the proposed approach made it possible to detect a number of phenomena that indicate a high  
34 probability of an imminent seismic event of significant magnitude. Thus, statistical methods are applicable not only within the  
35 framework of the Gutenberg-Richter theory (Gutenberg & Richter 1956; Amitrano 2012; Sanchez & Vega-Jorquera 2018),  
36 which makes it possible to assess the possibility of earthquakes of a given magnitude on medium-term, on the order of months  
37 and years, of time intervals, but also in relation to small, up to several hours, intervals before the onset of impending seismic  
38 events, which is close to the current time regime.

39 **2 Mathematical apparatus used in solving the objective**

40 The article introduces the assumption used in (Volvach et al. 2022a,b,c; Kogan et al. 2021; Kogan 2015) that any physical  
41 fields  $x(t)$  measured in seismically active regions can be written in the form

$$42 \quad x(t) = x_1(t) + x_2(t). \quad (1)$$

43 Here  $x_1(t)$  is the background noise associated with the influence of a set of ordinary phenomena and processes. Whereas the  
44 term  $x_2(t)$  is solely due to the impact of an impending seismic event. At the same time, the hypothesis about the weak statistical  
45 dependence of these two random variables (RV) is introduced into consideration.

46 As indicated in the Introduction, below we will consider the properties of magnetic field statistics. In this case, the entire  
47 measurement period is divided into implementation segments of one minute duration, and each such segment is assigned 60  
48 measuring counts (one per second). As in (Volvach et al. 2022), to each implementation segment is matched value of the  
49 statistical functional

$$50 \quad L(n) = \frac{A}{M} \sum_{l=n-(M-1)}^n |\mathcal{L}_l|, \quad \mathcal{L}_l = \sum_{m=0}^{N-1} (-1)^m P_{m,l}. \quad (2)$$

51 Here,  $M = 100$ , the factor  $A = 1000$  is necessary to obtain a convenient for analysis range of values  $L(n)$ ,  $l$  is the number of  
52 the implementation segment, the value  $n$  corresponds to the moment of observation, that is, the completion time of the  
53 implementation segment with this number, and  $P_{m,l}$  is the probability of the measured value of the function  $f[x(t)]$ ,  
54 corresponding to the indicated segment number  $l$ , falls into the  $m$ -th interval of the range of values of the form

$$55 \quad f[x(t)]_{min} + mh \leq f[x(t)] < f[x(t)]_{min} + (m + 1)h, \quad 0 \leq m \leq N - 1 \quad (3)$$

56 In (3)  $f[X] = \sin(X)$  (see<sup>2</sup>) and  $f[x(t)]_{min} \geq -1$  is the smallest value  $f[x(t)]$  for a given implementation segment. (The  
57  $x(t)$  values were measured and accepted in calculations in nT units.) In addition, in (3) the sampling interval is set equal to  $h =$   
58 0.1, therefore, in (2) and (3)  $N = 20$ . According to (Volvach et al. 2022a,b,c; Kogan et al. 2021; Kogan 2015), functional (2)  
59 essentially depends on the level of entropy of the values of the random process, the value of which significantly increases  
60 when an independent stochastic term  $x_2(t)$  appears in (1).

61 **3 Data and analysis of the properties of the functional  $L(n)$  constructed from the measurements of the magnetic field**

62 The International Real-time Magnetic Observatory Network - the global network of observatories, monitoring the Earth's  
63 magnetic field and the data are available as digital data files ([www.intermagnet.org](http://www.intermagnet.org), [ftp.seismo.nrcan.gc.ca](http://ftp.seismo.nrcan.gc.ca)).

64 Fig. 1 shows the dependence  $L(n)$ , constructed from measurements of the H-component of the magnetic field on June 24 and  
65 25, 2021, with a magnetometer at the above-mentioned test site of the CrAO in Katsiveli. Hereinafter, the horizontal axis  
66 corresponds to UTC time in minutes starting from  $n = M = 100 \text{ min}$  after the first moment of the first day of the considered  
67 48-hour time interval (see (2)). In all figures, the solid vertical red straight line (drawn at  $n = 2459 \text{ min}$ ) denotes the moment  
68 of the earthquake under consideration. Let us introduce a number of definitions, illustrating them with examples from Fig. 1.

69 1. We call the main extrema the set of points of maxima and minima of the dependence  $L(n)$ , which on the intervals of both  
70 increasing and decreasing corresponds to the variation  $\delta L$  of the values of this functional, satisfying the condition

71 
$$\delta L \geq 0.2 \Delta L_{\max} . \quad (4)$$

72 In (4),  $\Delta L_{\max}$  is the difference between the largest maximum and the smallest minimum of functional (2) from the start to the  
73 moment of the considered earthquake. At the same time, an additional condition is introduced that any point considered as the  
74 main extremum must be horizontally removed from any other point of the  $L(n)$  curve by at least 35 minutes. Here and below,  
75 unless the opposite condition is set, small-scale variations in the values of  $L(n)$  are not taken into account. This term will  
76 denote fluctuations that are much smaller in modulus than the right side of (4) and, at the same time, are small in amplitude  
77 and duration compared to the variation of the functional  $L(n)$  in the region of the corresponding extremum. Thus, local trends  
78 are rather large quasi-rectilinear segments of the  $L(n)$  dependence, the boundary points of which are extrema, horizontally  
79 separated by a given minimum distance from any other points of the curve  $L(n)$ . In addition, within the limits of each such  
80 section, there should be a quasi-constant rate of change of this dependence. In Fig. 1, the main extrema, in particular, are the  
81 points  $h, a, b, c, d, l, f, e, g, p$ .

82 2. We will call the sections of the dependence  $L(n)$ , which have the properties of quasi-monotonicity and quasi-constant rate  
83 of change (also neglecting small-scale variations), as local trends. We assume that they correspond to the  $\delta L$  variation  
84 satisfying (4). In this case, the geometric deviation of the points of the local trend from the segment of the straight line  
85 connecting the points of its beginning and end should not exceed 15% of the modulus of the difference between the values of  
86 the dependence  $L(n)$  at these points. We emphasize that for the main extrema defined above, the corresponding intervals  
87 of increase and decrease can also be considered as local trends. Examples of local trends in Fig. 1 are, for example, segments  
88  $a - b$ ,  $i - j$  and  $e - u$  of a given curve.

89 3. Let us denote as global extrema those points of maxima and minima of the dependence  $L(n)$ , which correspond to the largest  
90 or, correspondingly, the smallest values of it over an interval of at least 24 hours. Moreover, they should be located near the  
91 middle of such a time interval. Such a point is, for example, point  $q$ , see Fig. 1.

92 4. Let's call the set of the main and global extrema, as well as the boundary points of trends, the guide points.

93 5. We will call a channel a collection of two straight lines, each of which is drawn through two guide points, provided that the  
94 difference  $\Delta\alpha$  of the directions of these straight lines satisfies the constraint

$$95 \quad \Delta\alpha \leq 1.5^\circ. \quad (5)$$

96 Here and below, we assume that the angle  $\Delta\alpha$  corresponds to the condition of equality of the geometric dimensions of the  
97 length units of the vertical and horizontal axes. At the same time, in this article, in all the figures, the unit of the abscissa axis  
98 is slightly greater than the unit of the ordinate axis. The angle  $\Delta\tilde{\alpha}$  corresponding to these figures between the directions of the  
99 "shores" of any of the channels is related to  $\Delta\alpha$  by the ratio

$$100 \quad \Delta\alpha \leq 0.8 \Delta\tilde{\alpha}. \quad (6)$$

101 The duration of the channel's existence, that is, the time interval between the guide points through which its boundaries pass,  
102 must be at least 150 minutes.

103 For clarity, all the figures show straight lines strictly parallel to the channel boundaries. They have the same number as the  
104 corresponding border, but with an additional index «'» (for example, in Fig. 1, straight line  $I'$  is assigned a parallel straight  $I$ ).  
105 In order to achieve a low probability of random proximity of the directions of the channel boundaries, we introduce additional  
106 conditions. They are reduced either to the existence of one more (besides the channel boundaries) straight line satisfying (5)  
107 as applied to at least one of the channel banks, or to a significant overlap area (with respect to the abscissa axis) of the areas  
108 between the guide points through which these boundaries pass, or to the commensurability of the time intervals between both  
109 pairs of such points with half a day, or to a small (compared to the duration of the channel's existence) distance between the  
110 points of the beginning of the boundaries of the channels and / or between the points of their termination, etc.

111 In Fig. 1 for the channel created by straight lines  $I-2$  (hereinafter we will introduce the designations of the form "channel  $I-2$ ") the angle  $\Delta\tilde{\alpha} \ll 1.0^\circ$ , and for channels  $3-4$  and  $5-6$  the value  $\Delta\tilde{\alpha} \approx 1.2^\circ$  and, accordingly,  $\Delta\tilde{\alpha} \approx 1.0^\circ$ . Taking into account  
112 (6), from here, for the angles  $\Delta\alpha$  corresponding to these channels, in this figure it follows that (5) is obviously fulfilled. Pairs  
113 of straight lines  $I-2$  and  $3-4$  are examples of spacing channels, and  $5-6$  is channel with substantially overlapping boundaries.  
114 Straight  $I$  and  $4$  are drawn through the guide points  $q, j$  and, respectively,  $i, d$ ; for the rest of the channel boundaries, the  
115 corresponding guide points are seen from Fig. 1.

116 6. We will call a sliding boundary (SB) any straight line that is drawn through two guide points and is tested by the curve  $L(n)$   
117 at two more points, one of which is also a guide (we will call it additional). The term "testing" means either a simple intersection  
118 of the curve (2) and a given straight line, or its passage from the guiding point at such a close distance that the deviation  
119 coefficient  $\delta$  satisfies the condition  
120

$$121 \quad \delta \leq 1.6\%, \quad (7)$$

122 where  $\delta = \frac{\Delta S}{L_g(n)} \cdot 100\%$ . Here  $\Delta S$  is the minimum vertical distance on the plane  $\{n, L(n)\}$  of the Cartesian variable between  
123 the straight line under consideration (both the SB and the channel boundary) and the given guide point, and  $L_g(n)$  is the value  
124 of the functional  $L(n)$  in this point.

125 An additional point can be located either between the two guides through which the SB line passes, or after them, but until the  
126 fourth test. In Fig. 1, the sliding border is straight line *l* drawn through the global extremum *q* and the guide point *j*. Point *m*  
127 is additional. Her area is highlighted with an orange ellipse. In this case, the coefficient  $\delta \approx 0.95\%$  satisfies (7).

128 7. We also define that if in the region of small-scale fluctuations there are more than three approximations of the curve  $L(n)$   
129 to the corresponding straight line when fulfilling (5), then any such segment of this curve will be assumed to correspond to  
130 one test.

131 Note that in Fig. 1, the variation value for the  $w - t$  segment of the  $L(n)$  curve is less than the right-hand side of (4) and  
132 therefore does not satisfy the definition of the local trend. It is also obvious that *w* is not the main or global extremum. In  
133 addition, at this point and its vicinity, the intersection of the curve under consideration and straight *l* does not occur. Therefore,  
134 despite the fulfillment of condition (7) for *w* (as applied to straight *l*), the point *w* is not included in the number of testing  
135 points.

136 Thus, straight line *l* is both the SB and the bank of the channel at the same time. Hereinafter, those channel boundaries that  
137 are not sliding boundaries will be denoted by dashed straight lines, and the SB themselves will be denoted by solid straight  
138 lines.

139 With regard to channel boundaries, an additional point, if any, can also be located either between those two guide points  
140 through which this boundary passes, or after them. In this case, for one channel boundary, there can be no more than three  
141 consecutive tests. If this rule is violated, any segment of the corresponding straight line containing the indicated three  
142 sequentially tested points is considered the channel boundary. (These three points include also and those two guide points  
143 through which the given channel boundary is drawn.)

144 We now turn directly to the search for the precursors of the earthquake under consideration. In Fig. 1, three vertical dashed  
145 straight lines in the right part of it are drawn from the points of the fifth testing of the curve  $L(n)$  of the bank lines of channels  
146 1–2, 3–4, and 5–6. (Here and below, similar vertical dashed straight lines mark the moments of time corresponding to the  
147 appearance of the "graphic precursors" considered below). In this case, the lower boundary of the first of these channels is  
148 assumed to be the segment  $q - j$  of straight line *l* containing an additional point *m*. The fact of the existence of such channels  
149 can be interpreted as the emergence of a set of deterministic processes immediately before an earthquake.

150 The time intervals from the indicated points of the fifth testing to the moment of the earthquake are  $T_{H,1} = 296 \text{ min}$ ,  $T_{H,2} =$   
151  $278 \text{ min}$  and  $T_{H,3} = 197 \text{ min}$ . As will be shown below, the phenomena of the fifth testing of the channel boundaries precede  
152 the considered seismic event and when carrying out a similar statistical analysis for the E- and Z- components of the measured  
153 geomagnetic field. Therefore, we will consider the moment of the indicated fifth testing as the time of realization of one of the  
154 types of "graphic precursors" of an impending earthquake.

155 In addition, as will be confirmed below, in the study of all three components of the magnetic field, the point of the fourth  
156 testing of the sliding boundary from the side of the curve  $L(n)$  is also a recurring precursor of an earthquake. This effect takes  
157 place in Fig. 1 at point *v* in relation to sliding border in the form of straight line *l*. (At this point, the indicated fourth testing

158 of this SB takes place, also marked with a vertical dotted straight line, see Fig. 1.) The appearance of SB can also be called the  
159 emergence of a deterministic phenomenon a few hours before the impending earthquake.

160 This condition, as well as all other restrictions specified in the article (see, in particular, (4) - (8)) are introduced in order to  
161 minimize the number of linear structures under consideration in the range from several units to about eight to ten. In this case,  
162 the conditions for analyzing the degree of concentration of the considered precursors over limited time intervals are  
163 significantly simplified. As follows from the results of this article, the beginning of the considered earthquake is preceded by  
164 a sharp increase in the concentration of these precursors over the last few hours.

165 Further, when analyzing the process of "final preparation" of a seismic event, as well as when determining the average duration  
166 of the interval from the moment of registration of a precursor to the onset of an earthquake, we will take into account only  
167 those precursors that are separated from the time of its onset by no more than an interval

$$168 \quad T_{max} = 720 \text{ min} \quad (8)$$

169 Therefore, ~~in this case~~, the time interval from point  $v$  in Fig. 1 и два подобных интервала от первых двух предвестников  
170 на Fig. 3 until the moment of the seismic event is not taken into account.

171 In Fig. 2 shows the dependence  $L(n)$  for the E-component of the magnetic field (data from the magnetometer in Katsiveli).  
172 Here, channels 1–2, 3–4 and 5–6 are drawn, for which the angles  $\Delta\alpha < \Delta\tilde{\alpha} \ll 1^\circ$  (see (5) and (6)). Segments  $a - b$ ,  $i - j$ ,  
173  $c - d$ ,  $e - f$ ,  $m - l$  and  $l - h$  (their boundaries contain all but  $q$ , the guide points through which all the indicated straight are  
174 drawn) satisfy the definition of local trends. For points  $q$  and  $e$ , the definitions of the main and, accordingly, global extremum  
175 are fulfilled.

176 In the region of small-scale fluctuations, marked with an orange ellipse, there are more than three approximations of the curve  
177  $L(n)$  to straight line 5 when (5) is fulfilled. According to definition VII introduced above, we consider that such a segment of  
178 this curve corresponds to one test. Taking this into account, we find that the specified straight is a sliding boundary, the fourth  
179 testing of which takes place at point  $g$ , see Fig. 2.

180 By analogy with Fig. 1, we assume that the points of the fifth testing of the channel boundaries of the curve (2) or the fourth  
181 testing of the line of the specified SB correspond to the time of realization of the "graphic precursors" of an impending seismic  
182 event. Therefore, also by analogy with Fig. 1, we postpone the intervals  $T_{E,1} = 434 \text{ min}$ ,  $T_{E,2} = 251 \text{ min}$ ,  $T_{E,3} = 231 \text{ min}$   
183 and  $T_{E,4} = 181 \text{ min}$  from the moments of the appearance of such precursors to the time of the beginning of this earthquake.

184 As in the previous case, in Fig. 2 these intervals correspond to green horizontal lines.

185 In Fig. 3 shows the dependence  $L(n)$  for the Z-component of the magnetic field (data from the magnetometer in Katsiveli).  
186 Here, channels 1–2 are drawn (here  $\Delta\tilde{\alpha} \approx 0.8^\circ$ ), as well as 2–3, 4–5 and 8–9, for which the angles  $\Delta\tilde{\alpha} \ll 1^\circ$  (see (5) and (6)).  
187 Note that straight 1, 2 and 3 are almost parallel. Sliding boundaries 4, 6 and 7 are drawn through the first and third (counting  
188 from the left) test points; areas of additional points are marked with ellipses. Here, the guide point  $a$ , through which this line  
189 passes, is the beginning of the local trend  $a - b$ . For SB 7, the region of small fluctuations within the corresponding ellipse is  
190 associated with one test. Taking into account (8) for SB 6 and 7, the intervals from the time of the fourth testing to the moment

191 of the earthquake are not considered. Intervals  $T_{Z,1} = 596 \text{ min}$ ,  $T_{Z,2} = 588 \text{ min}$ ,  $T_{Z,3} = 396 \text{ min}$ ,  $T_{Z,4} = 350 \text{ min}$  and  $T_{Z,5} =$   
192  $144 \text{ min}$  depicted by green horizontal lines.

193 For ease of comparison in Table 1 shows all the obtained values of the intervals  $T_H$ ,  $T_E$  and  $T_Z$  (first 5 lines), as well as their  
194 average values of the form  $\langle \dots \rangle_{720}$  and  $\langle \dots \rangle_{360}$  over the last 720 and, respectively, 360 minutes before the earthquake.

## 195 4 Discussion of the results

196 The results presented in this paper rely on data collected at magnetic observatories. We used the INTERMAGNET stations -  
197 the global network of observatories, monitoring the Earth's magnetic field ([www.intermagnet.org](http://www.intermagnet.org)).

198 As a result of analyzing the statistics of magnetic field measurements carried out in the last two days before the earthquake,  
199 which occurred at 18:28:37 (UTC) on June 25, 2021, 8 kilometers from the city of Yayladere (Turkey), we come to the  
200 following conclusions.

201 External forcing influences geomagnetic data. The analysis on the geomagnetic observations consider the solar forcing. In  
202 Fig.4 shows the K-index of solar radiation changes during the period 00:00:00 on 24.06.2021 – 23:59:59 on 26.06.2021. As  
203 can be seen from the chart, the K-index was in the quiet (green) zone.

204 1. In the last hours before a given seismic event, there is an effect of concentration of recurring deterministic phenomena  
205 identified in the previous section of the article and interpreted as a kind of "graphic precursors" of an impending seismic event.

206 In this case, for all three components of the geomagnetic field, a kind of "ladder of precursors" appears, see Fig. 1 – 3.

207 2. The most common precursor is the phenomenon of fivefold dependency testing (2) of the boundaries of the channels defined  
208 above. These channels are formed by a pair of almost parallel straight lines (see (5)), which limit the values of the  $L(n)$  curve  
209 for at least 150 minutes.

210 3. Sliding boundaries in the form of straight lines, each of which is tested at least four times by the dependence in question, is  
211 also an essential type of "graphical precursor". In this case, the first three tests of this kind must correspond to topologically  
212 selected points of the curve (2).

213 4. As follows from the analysis of the data in Table 1, in the last 6 hours before the event, the values of the intervals  $T_H$ ,  $T_E$   
214 and  $T_Z$  are comparable. In particular, this manifests itself in the relative closeness of the average values  $\langle T_H \rangle_{360}$ ,  $\langle T_E \rangle_{360}$  and  
215  $\langle T_Z \rangle_{360}$ , which correspond to averaging over the last 360 minutes before the onset of this earthquake. As the authors believe,  
216 this fact is an argument in favor of the reliability of the proposed method.

217 5. The discovered effects of the existence of deterministic phenomena in the form of channels and sliding boundaries are quite  
218 reliable (outside the scope of this work, they were tested on a large array of data on various earthquakes and corresponding  
219 measurements of fields of a very different nature), but at the same time they are difficult to explain. It is possible that the  
220 existence of such straight linear boundaries of the values of functional (2) is associated with an almost constant (on a 48-hour  
221 scale) speed of movement of lithospheric plates; this assumption is completely hypothetical. In addition, significant difficulties  
222 in explaining the discussed phenomena can be associated with poor theoretical knowledge of the area of probability theory

223 corresponding to the phenomena under consideration, which can be attributed to "anti-Gaussian" random processes associated  
224 with the properties of the sum of a large number of strongly dependent random variables.

225 **6. The study of the influence of cracks on various physical properties of rocks is one of the main tasks of earthquake prediction.**  
226 The conductivity of natural media is due to the transfer of electric charges by the through current of electrons, ions, holes. In  
227 the epicenter of an earthquake, in addition to an increase in the number and length of elementary cracks, their closure and the  
228 appearance of a main crack, there is also a change in the electrical resistance of rocks. When the soil level and density change,  
229 the specific electrical conductivity of rocks changes by several orders of magnitude compared to the initial value, which leads  
230 to a change in the characteristics of the magnetic field.

231 With the help of the INTERMAGNET international network, the Earth's magnetic field is monitored, which makes it possible  
232 to create a technique that can be used to predict seismic processes in various regions of the world in close to real time.

233 **7. Note that Volvach et al. 2022a,b,c,d; Volvach et al. 2023a, using an approach similar to that used in this article, precursors**  
234 for 37 earthquakes are considered. For 26 of them (with the exception of aftershocks that are not far removed in time from the  
235 previous event), almost all of the considered precursors are recorded before their "own" earthquake at a time interval of no  
236 more than 20–25% of the total considered measurement period  $\Delta t_{\text{glob}}$ . Outside a given period of time, the number of such  
237 phenomena is much less than within it. Moreover, in the absolute majority of the cases under consideration, this interval is on  
238 the order of 5–10% or less of  $\Delta t_{\text{glob}}$ . The same effect also takes place in relation to the present article, which indicates the  
239 stability of the results of the method used. This fact means a high probability that the statistical effects under consideration are  
240 related precisely to the process of the "final preparation" of the approaching earthquake.

241 **8. As follows from this article, as well as Volvach et al. 2022a,b; Volvach et al. 2023a, if at least 3 considered precursors occur**  
242 within an interval of 300 minutes or more, according to the measurement statistics of at least one of the magnetic field  
243 components, the probability that an earthquake will occur within an interval of about an hour after the registration of the last  
244 specified precursor is very high. We emphasize that this conclusion is obviously preliminary, subject to verification in the  
245 course of further studies and relating to the case of a total duration of the analyzed measurement period of the order of two  
246 days.

247 **9. Note that the relative closeness of the mean values of the considered time intervals corresponding to different components**  
248 of the magnetic field (see Table 1) is an argument in favor of the stability of the applied approach. Which in turn makes it  
249 possible to speak about the objectivity of the results obtained.

250 We also point out that the different time of occurrence of precursors in the analysis of the statistics of different components of  
251 the magnetic field can be explained by different amplitudes of the random process  $x_2(t)$  for each of the components of this  
252 field. Such spatial anisotropy can be associated, in particular, with the existence of distinguished directions for the development  
253 of cracking in the zone of preparation of a seismic event. The consequence of this difference in amplitudes is a different degree  
254 of averaging of fluctuations in the probability density of the background noise for different components of the magnetic field.  
255 This effect manifests itself both in the noncoinciding form of the  $L(n)$  curves corresponding to different components of the  
256 magnetic field, and in different times and in the number of detected precursors. In this case, the indicated proximity of the

257 average values of the indicated time intervals corresponding to various components of the magnetic field can be explained by  
258 a synchronous change in the properties of the statistics of all components of the magnetic field, the moments of the beginning  
259 and/or completion of the next stage of the "final preparation" of the approaching event. Thus, such a difference in the time of  
260 registration of individual precursors under consideration for different field components, in combination with a small relative  
261 difference in the corresponding average values, is quite consistent with the logic of the calculations.

262 10. We also note that, according to the statistical meaning of the functional  $L(n)$ , its maxima and minima with high probability  
263 correspond to the smallest and, accordingly, the largest level of variations of the random process  $x_2(t)$ , independent or weakly  
264 dependent on background noise, as applied to a local sequence from  $M$  segments of realization, see (2), which precede the  
265 given moment of time. The article introduces the hypothesis that such an independent or quasi-independent process is  
266 determined by a set of phenomena associated with the fracture of lithospheric plates in the area of preparation for an  
267 approaching earthquake. (It is taken into account that there are no significant geomagnetic disturbances associated with solar  
268 events during the period under study.) Therefore, if this hypothesis is true, the maxima and minima of the dependence  $L(n)$   
269 correspond to the minimum and, accordingly, the maximum values of the level of compression of lithospheric plates in the  
270 region of the future hypocenter.

271 Therefore, the appearance of a channel means the appearance of boundaries determined by deterministic or quasi-deterministic  
272 functions of time, within which the process of oscillations of the corresponding seismic pressure occurs. Similarly, the  
273 formation of a sliding boundary means the existence of such a limit, limiting from above or below the values of the specified  
274 pressure. It is in this sense that the term about the occurrence of deterministic phenomena used in this article should be  
275 considered.

276 We also note that, taking into account the definition and properties of the functional  $L(n)$ , the linear form of the boundaries of  
277 the indicated graphical objects, whether they be channels or sliding boundaries, can correspond to the hyperbolic form of quasi-  
278 deterministic time dependences that determine the boundaries of seismic pressure fluctuations during the "final preparation"  
279 period approaching earthquake. The validity of this assertion will be investigated in future works.

280 Taking into account the foregoing, let us additionally explain the physical meaning of the chosen criteria for registering the  
281 precursors of an approaching earthquake. The fifth test of the curve  $L(n)$  of the boundaries of any of the channels means either  
282 a double "internal" oscillation within the boundaries of this channel (with the possibility of going beyond its limits at the point  
283 of the fifth test, see channel 5–6 in Fig. 1). This means a double approach of the seismic pressure level to some time-varying  
284 critical level, which is determined by a quasi-deterministic dependence, with the possibility of its "breakthrough" in the end.  
285 Or such a five-time test means from four to five consecutive "attempts to break through" (either only from above, or only from  
286 below) both boundaries of a given channel (see channel 1–2 in Fig. 1), also with the possibility of going beyond its limits  
287 during the last test. The physical meaning of such behavior of the  $L(n)$  curve is reduced to five successive approaches of the  
288 seismic squeezing level to a certain critical level, which is also determined by a quasi-deterministic function of time. As follows  
289 from Volvach et al. 2022a, in both cases, such phenomena with a fairly high probability take place at the "final preparation"  
290 stage of the forthcoming earthquake.

291 The physical meaning of the criterion for registering precursors after the fourth test of the  $L(n)$  curve of the sliding boundary  
292 line is similar. It comes down to identifying at least four consecutive facts of reaching a certain time-varying critical level,  
293 which is determined by a quasi-deterministic dependence, with the possibility of its “pushing through” as a result. Also  
294 according to Volvach et al. 2022a, such effects with a fairly high probability occur in a fairly short, on average, about several  
295 hours, time interval before the onset of the upcoming earthquake.

## 296 **5 Conclusions**

297 In the article, based on the analysis of the results of measurements of the geomagnetic field, the deterministic phenomena  
298 associated with the process of "final preparation" of the earthquake with a magnitude of 5.4, which occurred on June 25, 2021,  
299 near the Turkish city of Yayladere, were considered. Based on the results obtained, "graphic precursors" were identified in the  
300 form of repeating phenomena of the emergence of channels and sliding boundaries, the properties of which were investigated  
301 in this work. The authors consider the most promising direction of further research to determine, within the framework of the  
302 methodology proposed in the article, not only the time, but also the coordinates of the future epicenter, and, possibly, the  
303 magnitude of the expected earthquake.

## 304 **Data availability statement**

305 The data underlying this paper are available in the paper and through the electronic resources: [www.intermagnet.org](http://www.intermagnet.org),  
306 [ftp.seismo.nrcan.gc.ca](ftp://ftp.seismo.nrcan.gc.ca).

## 307 **Acknowledgments**

308 The results presented in this paper rely on data collected at magnetic observatories. We thank the national institutes that support  
309 them and INTERMAGNET for promoting high standards of magnetic observatory practice ([www.intermagnet.org](http://www.intermagnet.org)).

## 310 **References**

311 Amitrano, D.: Variability in the power-law distributions of rupture events, how and why does b-value change. *Eur Phys J-Spec.*, 205, 199–215, <https://doi.org/10.1140/epjst/e2012-01571-9>, 2012.

312 Gutenberg, B., Richter, C.F.: Magnitude and energy of earthquakes. *Annali di Geofisica*, 9, 1–15, 1956.

313 Hasanov, A.A., Keramova, R.A.: Reflection of global geodynamical processes in seismic-geo-chemical mode of fluids of  
314 Azerbaijan at the example of catastrophic earthquake in the Indian ocean (26.12.04; MLH =8.9). In the book *Geophysics of*  
315 *XXI century*: 2005, M. collected papers of GEON. “Scientific world”. pp 326-330, 2006.

317 Lyubushin, A.A.: Micro-seismic noise in a minute's diapason of periods: properties and possible forecasting features. Physics  
318 of the Earth, 4, 17-34, DOI: 10.1134/S1069351308040022, 2008.

319 Khain, V.Y., Khalilov, E.N.: Space-time regularities of seismic and volcanic activities. Bulgaria, Burgas, SWB. p 304, 2008.

320 Kogan, L.P.: Change in statistical functionals of critical frequency prior to strong earthquakes. Geomagnetism and Aeronomy,  
321 45(3). 507-520, doi:10.1134/S0016793215040064, 2015.

322 Kogan, L.P., Bubukin, I.T., Shtenberg, V.B.: To the question of calculating the probability of strong earthquakes in real time.  
323 Chaos, Solitons and Fractals, 145. 110807, doi: 10.1016/j.chaos.2021.110807, 2021.

324 Sanchez, E., Vega-Jorquera, P.: New Bayesian frequency-magnitude distribution model for earthquakes applied in Chile.  
325 Physica A: Stat. Mech. and its Appl, 508, 305-312, 2018.

326 Sobolev, G.A., Lyubushin, A.A., Zakrjevskaya, N.A.: Asymmetric impulses, periodicity and synchronization of low-frequency  
327 microseisms. Volcanology and seismology, 2, 135-152, 2008.

328 Volvach, A.E., Kogan, L.P., Kanonidi K.H., Nadezhka, L.I., Bubukin I.T., Shtenberg, V.B., Gordetsov A.S., Krasnikova O.V.,  
329 Kislitsyn D.I.: Changes in the properties of the statistics of physical and biophysical fields as earthquake precursor,  
330 Communications in Nonlinear Science and Numerical Simulation, 108. 106200, doi: 10.1016/j.cnsns.2021.106200, 2022a.

331 Volvach, A., Kogan, L., Kanonidi, K., Nadezhka, L., Bubukin, I., Boborykina, O., Shtenberg, V. & Biazitov, D.: On the  
332 statistical precursors that preceded the earthquake of magnitude 6.0 on September 27, 2021, on the island of Crete. Arabian  
333 Journal of Geosciences. 15, 1358, doi: 10.1007/s12517-022-10656-8, 2022b.

334 Volvach, A.E., Kogan, L.P., Kanonidi, K.H., Bubukin, I.T., Shtenberg, V.B., Volvach, L.N., Biazitov, D.T.: Statistical  
335 precursors of a strong earthquake on April 6, 2009 on the Apennine Peninsula. Heliyon, e10200, doi:  
336 10.1016/j.heliyon.2022.e10200, 2022c.

337 Volvach, A.E., Kogan, L.P., Kanonidi, K.H., Nadezhka, L.I., Bubukin, I.T., Boborikina, O.V., Shtenberg, V.B., Biazitov, D.T.:  
338 A Possible Relationship between the Sets of Quasi-Linear Local Trends Statistically Detected in the Variations of the Magnetic  
339 Field Parameters before Earthquakes in Seismically Active Zones of the Black Sea, Caucasus, and Western Asia. Geodynamics  
340 & Tectonophysics 13 (5), 0680. doi:10.5800/GT-2022-13-5-0680, 2022d.

341 Volvach, A., Kogan, L., Kanonidi, K., Bubukin, I., Shtenberg, V., Volvach, L.: About Statistical Precursor Earthquakes on  
342 October 12, 2021 with a Magnitude of 6.4 on the Island of Crete. Romanian Journal of Physics. 68, 801, 2023.

343

344

345

346

347

348

349

350

351  
352  
353  
354  
355

356 **Table 1. Values of intervals from the time of realization of «graphic precursors» to the moment of the beginning of the**  
357 **earthquake, as well as their averaging.**

358  
359  
360

<i>I</i>	<i>T<sub>H,i</sub>, min</i>	<i>T<sub>E,i</sub>, min</i>	<i>T<sub>Z,i</sub>, min</i>
1	296	434	596
2	278	251	588
3	197	231	396
4		181	350
5			144
$\langle \dots \rangle_{720}$	257	274	414
$\langle \dots \rangle_{360}$	257	221	297

361  
362  
363  
364  
365  
366  
367  
368  
369  
370  
371  
372  
373

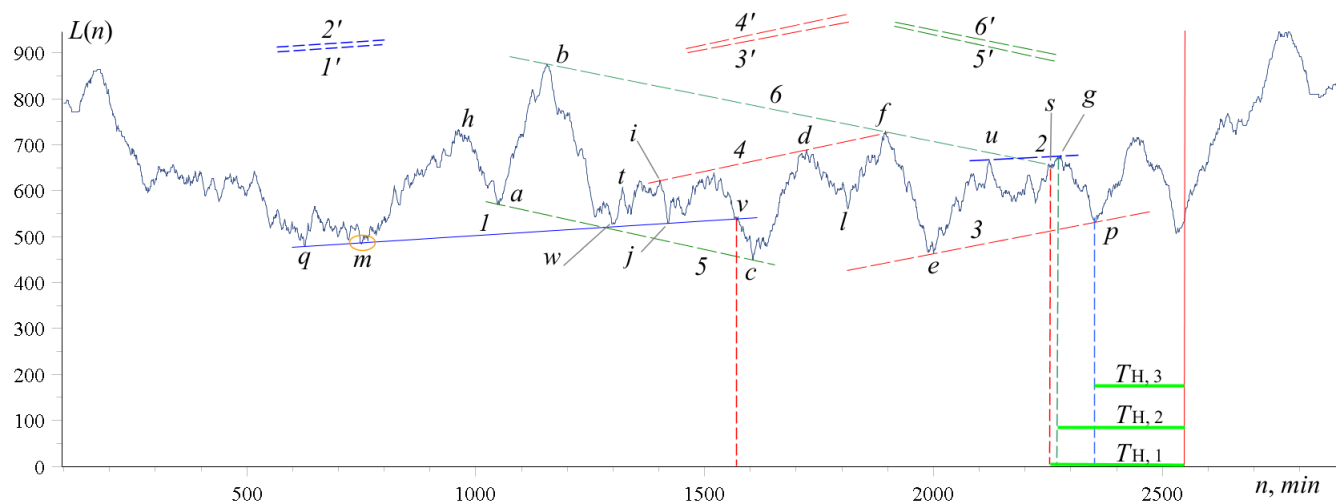
374

375

376

377

378



379

380 **Figure 1. Dependence  $L(n)$  for the H-component of the magnetic field from measurements at the Katsiveli.**

381

382

383

384

385

386

387

388

389

390

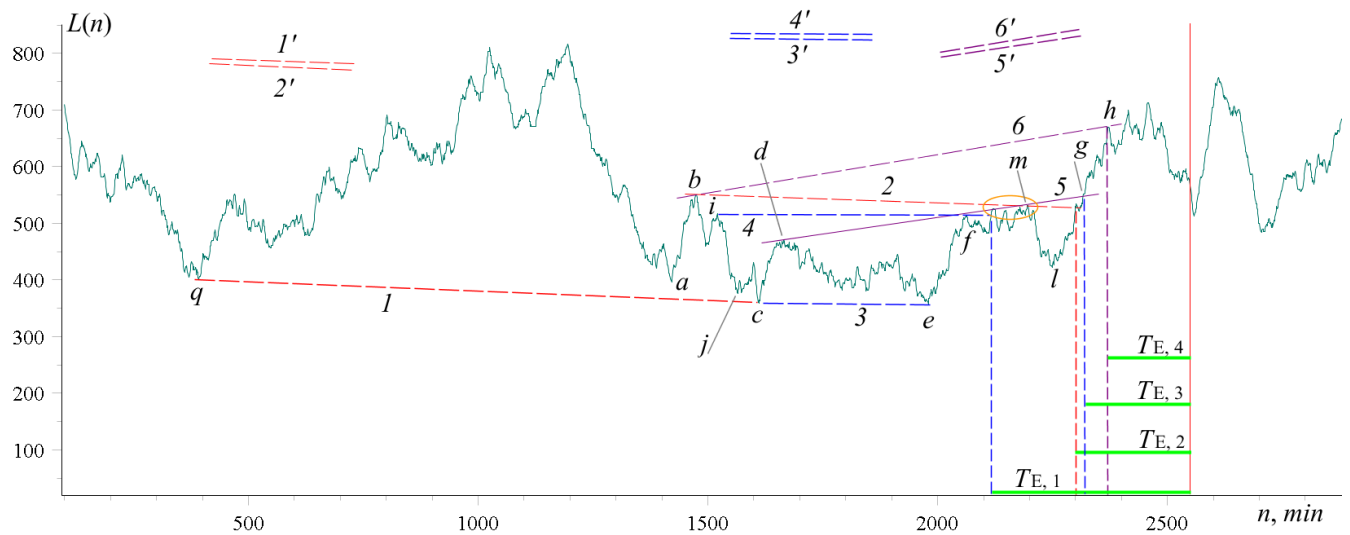
391

392

393

394

395



396

397 **Figure 2. Dependence  $L(n)$  for the E-component of the magnetic field from measurements at the Katsiveli.**

398

399

400

401

402

403

404

405

406

407

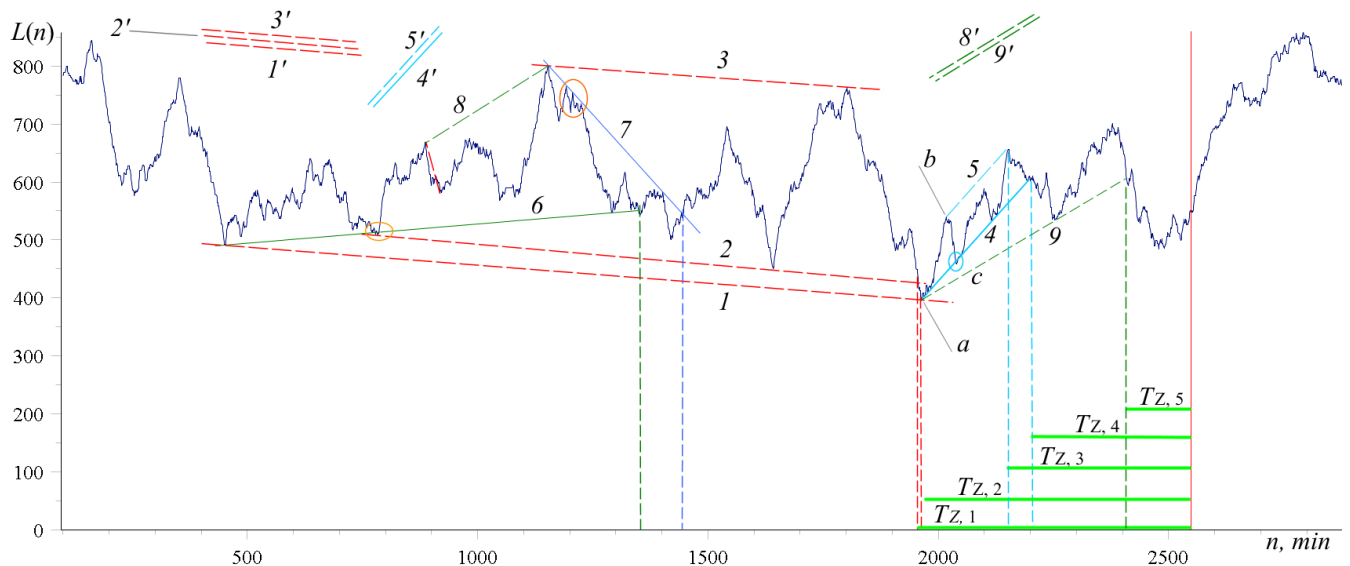
408

409

410

411

412



413

414 **Figure. 3. Dependence  $L(n)$  for the Z-component of the magnetic field from measurements at the Katsiveli.**

415

416

417

418

419

420

421

422

423

424

